

Nonlinear feedback control of the wake past a plate with a suction point on the downstream wall

By LUCA CORTELEZZI

Department of Mechanical and Aerospace Engineering,
University of California, Los Angeles, CA 90095-1597, USA

and Department of Mathematics,
University of California, Los Angeles, CA 90095-1555, USA
e-mail: crtlz@math.ucla.edu

(Received 24 April 1995 and in revised form 11 April 1996)

Active circulation control of the two-dimensional unsteady separated flow past a plate with a suction point on the downstream wall is considered. The rolling-up of the separated shear layer is modelled by a pair of point vortices whose time-dependent circulation is predicted by an unsteady Kutta condition. A nonlinear controller able to confine the wake to a single vortex pair of constant circulation is derived in closed form for any free-stream condition. Dynamical system analysis is used to explore the performance of the controlled system. Finally, the control strategy is applied to three different classes of unsteady flows and the results are discussed.

1. Introduction

Active control of unsteady separated fluid flows is attracting wide interest in both the fluid mechanics and control communities because of the many potential engineering applications. See Gad-el-Hak & Bushnell (1991) for a discussion and references. Drag reduction, lift enhancement, noise and vibration control, mixing improvement, etc. are some of the many problems where active control of flows past bluff bodies finds natural applications.

The problem of actively controlling an unsteady fluid flow is in general nonlinear. Since the control of nonlinear systems remains a research topic, there is no general framework to obtain a desired controller. However, it is well known that the model chosen to represent the plant is of crucial importance in the derivation of the controller. A very complex and detailed model, the full Navier–Stokes equations for example, might generate an overly complex controller or might make the derivation of the controller impossible. On the other hand, an over-simplified or linear model facilitates the derivation of the controller but might generate a controller unable to achieve the desired control objective. A reasonable compromise is a reduced model able to capture the dynamic features of the flow that one wants to control. See Cao & Aubry 1993, Rajaei, Karlsson & Sirovich 1994, Cortelezzi, Leonard & Doyle 1994. Typically, the reduced model is a low-dimensional nonlinear system governed by a set of ordinary differential equations, while the real flow has infinite dimensions. An advantage of working with a reduced model is that one can use dynamical system analysis to investigate the problem. Analysis of the phase space of the reduced system provides information about fixed points, limit cycles, bifurcation points, etc., characteristic of the flow un-

der consideration and consequently provides information about the effectiveness and robustness of the controller. Another advantage of model reduction is the potential for producing fast numerical algorithms which are essential for controlling a real flow.

Before attempting to control a laboratory flow one should take the intermediate step of controlling the same class of flows simulated by a more sophisticated CFD (Computational Fluid Dynamics) code. The application of the controller derived for the reduced model to a complex model should be successful if the two models are dynamically equivalent, i.e. if the phase spaces of the two models are topologically equivalent. The equivalence of the two models can be investigated via dynamical system and time series analysis. There are many advantages in controlling a flow simulated by another CFD code. All the flow quantities required by the controller to command the actuator can be easily measured. The action of the controller is automatically synchronized with the evolution of the flow because both algorithms run in virtual time. Furthermore, the controller can be tested on gradually more complex flows. For example, if the controller were derived for an inviscid model, then it could be applied to the same flow when the fluid is slightly viscous. In general the controller has to be made robust with respect to the perturbations introduced by the new environment, e.g. viscosity, three-dimensionality, background noise (see Doyle, Francis & Tannenbaum 1992; Fan, Tits & Doyle 1991). Only an iteration process might produce a controller able to handle the flow simulated by the Navier–Stokes equations. Finally, the control of a laboratory flow can be attempted when the controller generated by this chain of refinements is robust enough to perform in the presence of the unmodelled and unpredictable uncertainties affecting the real system and is fast enough to control the flow in real time.

Recently, efforts to modify certain features of the wake behind bluff and slender bodies, such as reduction or magnification of the wake thickness (Tokumaru & Dimotakis 1991), wake stabilization (Roussopoulos 1993), vortex cancellation (Koochesfahani & Dimotakis 1988), pattern reproduction (Ongoren & Rockwell 1988*a,b*; Gopalkrishnan *et al.* 1994), and lift enhancement (Rossow 1977; Slomski & Coleman 1993) have been successful. In all these investigations the free-stream velocity was kept constant and quasi-steady results were achieved usually by moving the body or the actuator with a frequency scaled by the shedding frequency. In a more general situation in which the free-stream velocity is time dependent this approach is generally not sufficient to control the flow and a nonlinear control strategy is necessary.

The present study investigates the active control of the wake past a plate perpendicular to an unsteady fluid flow. This problem has been previously studied by Shermer (1992) in the viscous case for a constant free-stream velocity, and by Cortelezzi (1993) and Cortelezzi *et al.* (1994) in the inviscid case for an unsteady free-stream velocity when the length of the plate is finite and semi-infinite respectively. In all studies the control objective was the suppression of the vortex shedding: Shermer achieved control by applying a body force, while Cortelezzi and Cortelezzi *et al.* achieved control by changing the length of the plate. All the control strategies showed some weaknesses. The global body force used by Shermer cannot be realistically applied in most situation, while the controllers derived by Cortelezzi and Cortelezzi *et al.* were able to suppress the vortex shedding only over a finite time. The present investigation derives in closed form a nonlinear controller able to confine the wake to a single vortex pair of constant circulation over any interval of time using as an actuator a suction point on the downstream wall of the plate.

In §2, we model the unsteady separation from the tips of a flat plate by means of a pair of point vortices whose time-dependent circulation is predicted by an unsteady

Kutta condition (Brown & Michael 1954; Rott 1956; Cortelezzi 1993; Cortelezzi *et al.* 1994). The problem is further simplified by imposing wake symmetry. The motion of the vortex pair is determined by a nonlinear ordinary differential equation first proposed by Brown & Michael in 1954. A suitable vortex shedding mechanism is also introduced to allow the simulation of flows involving multiple vortices. This reduced model is able to capture the main features of the flow and, for example, is quite accurate for power-law starting flows. See Cortelezzi (1993) for the validation of the model with respect to experimental and numerical results.

In §3, we consider as a control actuator a suction point placed on the downstream wall of the plate. The control objective is to confine the wake to a single vortex pair of constant circulation. We show that suction is a very efficient means to control the production of circulation. Thanks to the simplicity of the model we obtain for any time-dependent free-stream velocity the analytical closed-form solution of the controller, i.e. the predicted suction necessary to inhibit the production of circulation when a vortex pair is present in the flow.

In §4, we perform an analysis of dynamical system type to characterize the performance of the controller. When the free-stream velocity is constant, we show the existence of fixed points for the unperturbed system and compute the locus of the fixed points. There is a critical value for the circulation associated with the vortex pair above which one can find two pairs of fixed points: a pair of stable nodes and a pair of saddle points farther downstream. The circulation plays the role of a bifurcation parameter and the vector field undergoes a saddle-node bifurcation when the circulation is near its critical value. The analysis of the phase space shows the existence of a controllable region between the plate and the stable manifolds of the saddle points. When the free-stream velocity oscillates periodically about a unit mean, we compute the Poincaré section to characterize the perturbed system. We show the topological equivalence between the Poincaré section and the phase space of the unperturbed system. The stable node of the Poincaré section represents a limit cycle while the saddle point represents an unsteady periodic orbit.

In §5, we present the results of three simulations. The first two simulations document the ability of the controller to drive the vortex pair to the stable nodes when the free-stream velocity is constant or to a limit cycle when the free-stream velocity oscillates periodically. The third simulation documents the performance of the controller when the free-stream velocity oscillates pseudo-randomly.

2. Mathematical formulation

In this section we introduce a mathematical model of the two-dimensional unsteady separation from the tips of a finite plate with a suction point of strength s at the centre of the downstream wall. Let us assume that the regions of vorticity that separate from the boundary layer and are convected away are thin enough to justify a description by means of a vortex sheet. The consequent stretching and rolling up of the vortex sheet, due to the unsteadiness of the flow, suggests replacing the spirals with point vortices. However, the vortex sheet which represents the separating boundary layer is not completely lost. It connects the separation point to a point vortex of variable circulation which is able to satisfy an unsteady Kutta condition. Furthermore, it is assumed to be of negligible circulation with respect to the circulation of the point vortex. The mathematical representation of the feeding vortex sheet is simply the branch cut due to the logarithmic singularity representing the vortex. All the other vortices in the wake are represented by point vortices of fixed circulation.

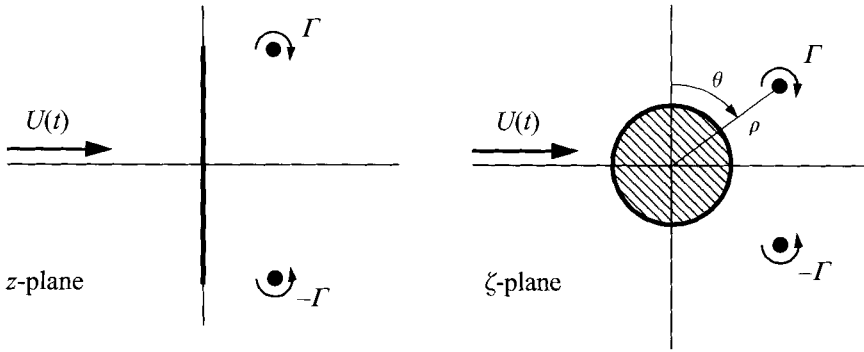


FIGURE 1. Physical and mapped planes for the flow past a flat plate.

We choose, for simplicity, a frame of reference fixed to the plate so that the body can be identified with the segment $[-2ia, 2ia]$ and the suction point s coincides with the point $(0^+, 0)$. Then, the flow of an incompressible irrotational fluid about such a body can be analysed via conformal mapping. Using the Joukowski transformation

$$z = \zeta - \frac{a^2}{\zeta}, \quad (2.1)$$

we map the finite plate of length $L = 4a$ in the z -plane onto the circle of radius a in the ζ -plane (see figure 1), preserving the characteristic of the flow at infinity.

To make the problem dimensionless we have to define a characteristic length and time scale. For this purpose we write the free-stream velocity as follows:

$$U(t) = U_\infty + u(t), \quad (2.2)$$

where U_∞ is the unperturbed free-stream velocity and $u(t)$ is the time-dependent component. If we choose the circle radius as characteristic length and a/U_∞ as characteristic time of the problem then we can define the following dimensionless quantities:

$$\left. \begin{aligned} z^* &= \frac{z}{a}, & \zeta^* &= \frac{\zeta}{a}, & a^* &= 1, & t^* &= \frac{U_\infty t}{a}, \\ U^* &= \frac{U}{U_\infty} = 1 + \epsilon_U, & \Gamma^* &= \frac{\Gamma}{U_\infty a}, & s^* &= \frac{s}{U_\infty a}. \end{aligned} \right\} \quad (2.3)$$

where Γ is the circulation. Note that $\epsilon_U = u/U_\infty$ contains the unsteadiness of the free-stream velocity and is not necessarily small with respect to unity. From this point on, we continue the mathematical formulation of the problem using dimensionless variables, where the stars are omitted for convenience.

There is experimental evidence (D. L. Lisosky 1993, private communication) that the near wake is nearly two-dimensional and symmetric about the x -axis if the plate moves with a non-zero acceleration. Under these circumstances the problem can be simplified by imposing symmetry with respect to the real axis, i.e. by requiring that the vortices have equal and opposite circulation, Γ_n and $-\Gamma_n$, and are located in complex-conjugate positions, ζ_n and $\bar{\zeta}_n$, respectively. Since the velocity field has to satisfy Laplace's equation and the boundary condition in the mapped plane can be treated using the circle theorem, we can build the complex potential F by superimposing basic flows. Thus, the complex velocity field $w = dF/d\zeta$ has the form

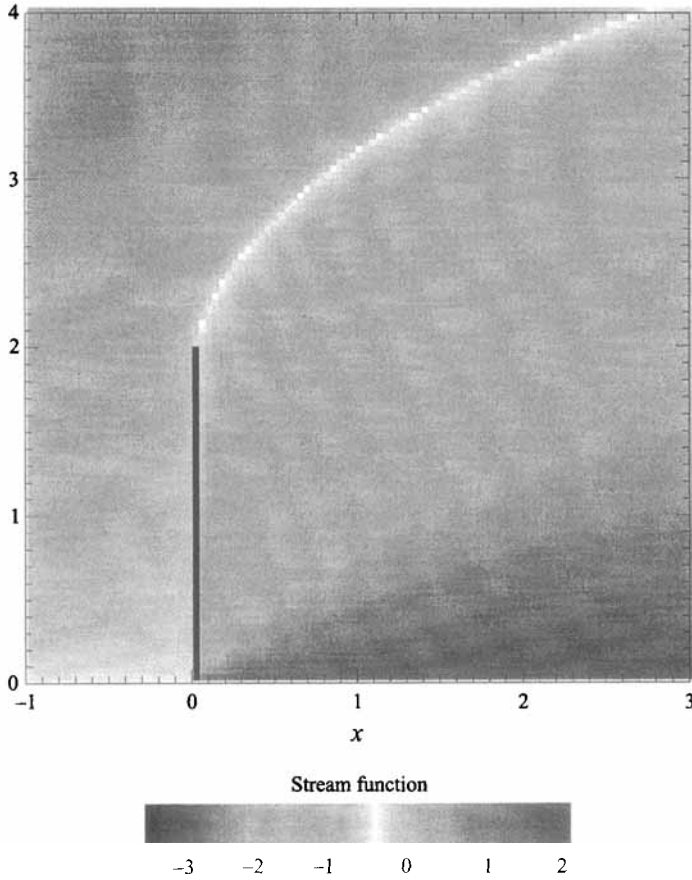


FIGURE 2. Instantaneous stream function, $s = -2U$.

$$\begin{aligned}
 w(\zeta, t) = & U \left(1 - \frac{1}{\zeta^2} \right) + \frac{i\Gamma_1}{2\pi} \left(\frac{1}{\zeta - \zeta_1} + \frac{\bar{\zeta}_1}{1 - \zeta\bar{\zeta}_1} - \frac{1}{\zeta - \bar{\zeta}_1} - \frac{\zeta_1}{1 - \zeta\zeta_1} \right) \\
 & + \sum_{n=2}^N \frac{i\Gamma_n}{2\pi} \left(\frac{1}{\zeta - \zeta_n} + \frac{\bar{\zeta}_n}{1 - \zeta\bar{\zeta}_n} - \frac{1}{\zeta - \bar{\zeta}_n} - \frac{\zeta_n}{1 - \zeta\zeta_n} \right) - s \frac{\zeta + 1}{\zeta(\zeta - 1)}. \quad (2.4)
 \end{aligned}$$

Note that for convenience we take the circulation to be positive when in a clockwise sense, contrary to the usual convention. Note also that the singularity on the back face of the plate behaves as a sink when $s > 0$ and as a source otherwise. We impose the Kutta condition to regularize the potential flow at the tips of the plate. In the ζ -plane the flow is non-singular since the singularity has been absorbed by the mapping. To remove the singularity in the z -plane the complex velocity (2.4) in the mapped plane has to be zero at the top and bottom of the circle, i.e. at $\zeta = \pm i$. Solving for Γ_1 we obtain

$$\Gamma_1 = -\pi i \frac{(1 + \zeta_1^2)(1 + \bar{\zeta}_1^2)}{(\zeta_1 - \bar{\zeta}_1)(1 - \zeta_1\bar{\zeta}_1)} \left[2U - \sum_{n=2}^N \frac{i\Gamma_n (\zeta_n - \bar{\zeta}_n)(1 - \zeta_n\bar{\zeta}_n)}{\pi (1 + \zeta_n^2)(1 + \bar{\zeta}_n^2)} + s \right]. \quad (2.5)$$

Note that the circulation associated with the vortex pair depends on all the flow quantities, i.e. free-stream velocity U , suction s , position and circulation of all the vortex pairs, and the position of the vortex pair 1. The above expression suggests

that the Kutta condition can be satisfied even when there are no vortices in the flow. It suffices to choose $s(t) = -2U(t)$ (see figure 2).

To describe the motion of the vortex pair in the physical plane we use the following set of ordinary differential equations:

$$\frac{d\bar{z}_1}{dt} + (\bar{z}_1 + 2i) \frac{1}{\Gamma_1} \frac{d\Gamma_1}{dt} = \lim_{z \rightarrow z_1} \left\{ \frac{d}{dz} \left[F - \frac{i\Gamma_1}{2\pi} \log(z - z_1) \right] \right\}, \quad (2.6a)$$

$$\frac{d\bar{z}_r}{dt} = \lim_{z \rightarrow z_r} \left\{ \frac{d}{dz} \left[F - \frac{i\Gamma_r}{2\pi} \log(z - z_r) \right] \right\}, \quad (2.6b)$$

with the initial conditions:

$$\left. \begin{aligned} z_1(t_s) &= 2i, \\ z_r(t_s) &= z_{r_s}, \quad r = 2 \dots N. \end{aligned} \right\} \quad (2.7)$$

The term containing $d\Gamma_1/dt$ is known as Brown & Michael's correction (Brown & Michael 1954). The motion of the vortex of variable strength described by this equation guarantees no net force on the vortex and its connecting cut. The limit on the right-hand side, which represents the complex velocity at the vortex location without the self-induced contribution, produces the so-called 'Routh's correction' when it is evaluated in the mapped plane (e.g. Clements 1973).

We solve the problem in the mapped plane. Once we have performed the change of variables, substituted for the complex potential, and carried out the limit required in equation (2.6), we obtain

$$\begin{aligned} & \left[\frac{\bar{\zeta}_1^2 + 1}{\bar{\zeta}_1^2} + \frac{(\bar{\zeta}_1 + i)^2}{\bar{\zeta}_1} \frac{(1 + \zeta_1^2)(1 - \bar{\zeta}_1^2)}{(1 + \bar{\zeta}_1^2)(\zeta_1 - \bar{\zeta}_1)(1 - \zeta_1 \bar{\zeta}_1)} \right] \frac{d\bar{\zeta}_1}{dt} \\ & - \left[\frac{(\zeta_1 + i)^2}{\zeta_1} \frac{(1 - \zeta_1^2)(1 + \bar{\zeta}_1^2)}{(1 + \zeta_1^2)(\zeta_1 - \bar{\zeta}_1)(1 - \zeta_1 \bar{\zeta}_1)} \right] \frac{d\zeta_1}{dt} \\ & = \left(\frac{\zeta_1^2}{1 + \zeta_1^2} \right) \left\{ U \left(1 - \frac{1}{\zeta_1^2} \right) + \frac{i\Gamma_1}{2\pi} \left[\frac{\bar{\zeta}_1}{1 - \zeta_1 \bar{\zeta}_1} - \frac{1}{\zeta_1 - \bar{\zeta}_1} - \frac{\zeta_1}{1 - \zeta_1^2} \right] + \frac{i\Gamma_1}{2\pi} \frac{1}{\zeta_1(1 + \zeta_1^2)} \right. \\ & + \sum_{n=2}^N \frac{i\Gamma_n}{2\pi} \frac{(1 - \zeta_1^2)(\zeta_n - \bar{\zeta}_n)(1 - \zeta_n \bar{\zeta}_n)}{(\zeta_1 - \zeta_n)(\zeta_1 - \bar{\zeta}_n)(1 - \zeta_1 \zeta_n)(1 - \zeta_1 \bar{\zeta}_n)} - s \frac{\zeta_1 + 1}{\zeta_1(\zeta_1 - 1)} \left. \right\} \\ & - \frac{(\bar{\zeta}_1 + i)^2}{\bar{\zeta}_1} \left[2 \frac{dU}{dt} - \sum_{n=2}^N \frac{i\Gamma_n}{\pi} \left[\frac{1 - \zeta_n^2}{(1 + \zeta_n^2)^2} \frac{d\zeta_n}{dt} - \frac{1 - \bar{\zeta}_n^2}{(1 + \bar{\zeta}_n^2)^2} \frac{d\bar{\zeta}_n}{dt} \right] + \frac{ds}{dt} \right] \\ & \times \left[2U - \sum_{n=2}^N \frac{i\Gamma_n}{\pi} \frac{(\zeta_n - \bar{\zeta}_n)(1 - \zeta_n \bar{\zeta}_n)}{(1 + \zeta_n^2)(1 + \bar{\zeta}_n^2)} + s \right]^{-1}, \end{aligned} \quad (2.8a)$$

$$\begin{aligned} \frac{d\bar{\zeta}_r}{dt} &= \left[\frac{\zeta_r^2 \bar{\zeta}_r^2}{(1 + \zeta_r^2)(1 + \bar{\zeta}_r^2)} \right] \left\{ U \left(1 - \frac{1}{\zeta_r^2} \right) + \frac{i\Gamma_r}{2\pi} \left[\frac{\bar{\zeta}_r}{1 - \zeta_r \bar{\zeta}_r} - \frac{1}{\zeta_r - \bar{\zeta}_r} - \frac{\zeta_r}{1 - \zeta_r^2} \right] \right. \\ & + \frac{i\Gamma_r}{2\pi} \frac{1}{\zeta_r(1 + \zeta_r^2)} + \sum_{n \neq r}^N \frac{i\Gamma_n}{2\pi} \frac{(1 - \zeta_r^2)(\zeta_n - \bar{\zeta}_n)(1 - \zeta_n \bar{\zeta}_n)}{(\zeta_r - \zeta_n)(\zeta_r - \bar{\zeta}_n)(1 - \zeta_r \zeta_n)(1 - \zeta_r \bar{\zeta}_n)} - s \frac{\zeta_r + 1}{\zeta_r(\zeta_r - 1)} \left. \right\}, \end{aligned} \quad (2.8b)$$

with the initial conditions:

$$\left. \begin{aligned} \zeta_1(t_s) &= i, \\ \zeta_r(t_s) &= \zeta_{r_s}, \quad r = 2 \dots N, \end{aligned} \right\} \quad (2.9)$$

where Γ_1 is given by (2.5). Note that because of Brown & Michael's correction the equations are coupled not only through the position of the vortices but also through the velocity of the vortices.

The forces acting on the plate are of particular interest because they can be measured experimentally and are the crucial quantities in any problem involving the interaction between fluids and structures. The forces can be computed by means of the Blasius theorem, see Cheers (1979), Graham (1980), and Cortelezzi (1993) for different derivations. The drag has the following form:

$$D = 4\pi\rho \frac{dU}{dt} + 4\pi\rho \frac{ds}{dt} + i\rho \frac{d}{dt} \left[\frac{\Gamma_1(1 - \zeta_1\bar{\zeta}_1)(\zeta_1 - \bar{\zeta}_1)}{\zeta_1\bar{\zeta}_1} \right] + i\rho \sum_{n=2}^N \Gamma_n \frac{d}{dt} \left[\frac{(1 - \zeta_n\bar{\zeta}_n)(\zeta_n - \bar{\zeta}_n)}{\zeta_n\bar{\zeta}_n} \right]. \tag{2.10}$$

The component of the force along the imaginary axis, which represents the lift, is zero because of the imposed symmetry. The first term on the right-hand side is the force due to added mass, i.e. the inertia of the attached flow, while the second term is the contribution due to suction, and the last two terms are the contributions due to the evolution of the wake. We define the drag coefficient as follows:

$$C_D = \frac{D}{\frac{1}{2}\rho U_\infty^2 L}. \tag{2.11}$$

Note that the drag coefficient is well defined only in the case where the free-stream velocity is constant. In order to compute the drag coefficient in the unsteady cases that we present in §5, we choose for U_∞ the asymptotic value or the mean value of the free-stream velocity.

The final element necessary for a correct implementation of this model is a vortex shedding mechanism. If we envision the separation process by means of a vortex sheet, then the instantaneous circulation necessary to keep the flow regular at the tip of the plate is associated with an infinitesimal segment of the sheet which is shed in the fluid. Consequently, the circulation is distributed along the singular line and the sheet rolls up around the points of greatest absolute circulation per unit length, and it stretches most where the absolute circulation per unit length is smallest. As the process continues, we observe that a large amount of circulation concentrates in the core of the spirals which are connected to each other by filaments of almost negligible circulation. This process can be reflected in our model by replacing each spiral with a point vortex of fixed circulation, except for the spiral connected to the separation point which is replaced by a point vortex with time-dependent circulation. This latter vortex will continue to be fed circulation until the rate of change of circulation becomes zero because we conjecture that this is the part of the sheet that will be stretched the most.

Let us consider the problem of shedding a new vortex when $N - 1$ other vortices are already present in the flow. If t_s is the shedding time, then it is crucial to analyse the transition from t_s^- to t_s^+ . Up to the time t_s^- , the variable strength of vortex 1 satisfies the Kutta condition. At time $t = t_s$, the strength of this vortex is frozen and all the vortices are renumbered. Finally at t_s^+ a new vortex 1 is introduced into the flow to remove the square-root singularity. If we restrict our simulation to the case where the shed vortices have alternate sign, then we can model the vortex shedding by making the assumption that the time $t = t_s$ is determined by the condition

$$\left. \frac{d\Gamma_1}{dt} \right|_{t=t_s} = 0, \tag{2.12}$$

assuming $d^2\Gamma_1/dt^2|_{t=t_s} \neq 0$. Any other choice for the shedding time implies the arbitrary production of two sequential vortices of the same sign or the existence of a vortex whose strength decreases in time. The latter situation is physically unacceptable. This procedure has been proposed by Graham (1980) to simulate the flow induced by an oscillating diamond-shaped cylinder.

The quality of the simulation with many vortices depends in large part on the shedding mechanism. Let us assume that between two zero crossings $d\Gamma_1/dt$ is positive and has two peaks, then it is not clear whether one or two vortices should be shed during this period. It seems that the deepness of the trough separating the peaks would be an important parameter. If it is very deep it seems reasonable to have two vortices, otherwise one is sufficient. Although the shedding mechanism can be implemented for all cases, to avoid any ambiguity we restrict ourselves to cases where the rate of circulation production has only one local maximum or minimum between consecutive zero crossings or, equivalently, where $d^2\Gamma_1/dt^2$ does not change sign between crossings.

Because of the size and complexity of the problem we are not attempting to obtain an analytical solution. We solve the problem numerically using the methods described in our previous work (Cortelezzi 1993).

3. Active wake control

There are different approaches one can use to control the wake past a plate by suction. One can try to control the position of the vortices or some features of the velocity field. We choose to control the amount of circulation injected in the flow because we believe that this is the most efficient way to control the wake. To gain insight into the effectiveness of the suction as a mean to control the circulation, we compute the rate of circulation production by taking the time derivative of (2.5):

$$\begin{aligned} \frac{d\Gamma_1}{dt} = & -\frac{\pi i}{(\zeta_1 - \bar{\zeta}_1)(1 - \zeta_1 \bar{\zeta}_1)} \left[2U - \sum_{n=2}^N \frac{i\Gamma_n}{\pi} \frac{(\zeta_n - \bar{\zeta}_n)(1 - \zeta_n \bar{\zeta}_n)}{(1 + \zeta_n^2)(1 + \bar{\zeta}_n^2)} + s \right] \\ & \times \left[(1 + \bar{\zeta}_1^2)^2(1 - \zeta_1^2) \frac{d\zeta_1}{dt} - (1 + \zeta_1^2)^2(1 - \bar{\zeta}_1^2) \frac{d\bar{\zeta}_1}{dt} \right] \\ & - \pi i \frac{(1 + \zeta_1^2)(1 + \bar{\zeta}_1^2)}{(\zeta_1 - \bar{\zeta}_1)(1 - \zeta_1 \bar{\zeta}_1)} \left[2 \frac{dU}{dt} - \sum_{n=2}^N \frac{i\Gamma_n}{\pi} \left[\frac{1 - \zeta_n^2}{(1 + \zeta_n^2)^2} \frac{d\zeta_n}{dt} - \frac{1 - \bar{\zeta}_n^2}{(1 + \bar{\zeta}_n^2)^2} \frac{d\bar{\zeta}_n}{dt} \right] + \frac{ds}{dt} \right]. \end{aligned} \quad (3.1)$$

From the above expression we see that the rate of circulation production depends on all flow quantities and their derivatives. Note that suction and rate of change of suction contribute to the production of circulation in the same way as free-stream velocity and free-stream acceleration, respectively. Hence, using suction as a means to control the rate of circulation production is as powerful as using the free-stream velocity.

Our control objective is to inhibit the rate of circulation production after the starting vortex pair is shed in the flow. In other words, we want to predict the suction so that once the starting vortex pair is shed in the flow the Kutta condition remains satisfied without requiring a new vortex pair. The possibility of maintaining the wake confined to a controlled recirculating bubble has important implications for the problem of drag reduction in general. Moreover it can provide insight into vortex management techniques for the three-dimensional flow over a delta wing (see Rao 1987). Note that there is no conceptual difficulty in inhibiting the rate of circulation

production when more than one vortex pair is present in the wake, if it is required by the application under consideration.

Let t_s be the time when the starting vortex pair is shed in the flow, i.e. the time when the rate of circulation production is zero. Then for $0 \leq t \leq t_s$ the motion of the vortex pair of time-dependent circulation is prescribed by the following equation:

$$\begin{aligned} & \left[\frac{\bar{\zeta}_1^2 + 1}{\bar{\zeta}_1^2} + \frac{(\bar{\zeta}_1 + i)^2}{\bar{\zeta}_1} \frac{(1 + \zeta_1^2)(1 - \bar{\zeta}_1^2)}{(1 + \bar{\zeta}_1^2)(\zeta_1 - \bar{\zeta}_1)(1 - \zeta_1 \bar{\zeta}_1)} \right] \frac{d\bar{\zeta}_1}{dt} \\ & - \left[\frac{(\bar{\zeta}_1 + i)^2}{\bar{\zeta}_1} \frac{(1 - \zeta_1^2)(1 + \bar{\zeta}_1^2)}{(1 + \zeta_1^2)(\zeta_1 - \bar{\zeta}_1)(1 - \zeta_1 \bar{\zeta}_1)} \right] \frac{d\zeta_1}{dt} \\ & = \left(\frac{\zeta_1^2}{1 + \zeta_1^2} \right) \left\{ U \left(1 - \frac{1}{\bar{\zeta}_1^2} \right) + \frac{i\Gamma_1}{2\pi} \left[\frac{\bar{\zeta}_1}{1 - \zeta_1 \bar{\zeta}_1} - \frac{1}{\zeta_1 - \bar{\zeta}_1} - \frac{\zeta_1}{1 - \bar{\zeta}_1^2} \right] \right. \\ & \left. + \frac{i\Gamma_1}{2\pi} \frac{1}{\zeta_1(1 + \bar{\zeta}_1^2)} - s \frac{\zeta_1 + 1}{\zeta_1(\zeta_1 - 1)} \right\} - \frac{(\bar{\zeta}_1 + i)^2}{\bar{\zeta}_1} \left[2 \frac{dU}{dt} + \frac{ds}{dt} \right] [2U + s]^{-1} \end{aligned} \quad (3.2)$$

with the initial condition

$$\zeta_1(0) = i. \quad (3.3)$$

Note that suction appears in the above equation but in this study it is not used to manipulate the wake for $t \leq t_s$. In general, suction can be used to drive the system to some desired state at $t = t_s$, from which the controller that inhibits the production of circulation takes over.

When $t \geq t_s$ the equation of motion for the vortex pair of constant circulation $\pm \Gamma_1$, is

$$\begin{aligned} \frac{d\bar{\zeta}_1}{dt} = & \left[\frac{\zeta_1^2 \bar{\zeta}_1^2}{(1 + \zeta_1^2)(1 + \bar{\zeta}_1^2)} \right] \left\{ U \left(1 - \frac{1}{\bar{\zeta}_1^2} \right) + \frac{i\Gamma_{1s}}{2\pi} \left[\frac{\bar{\zeta}_1}{1 - \zeta_1 \bar{\zeta}_1} - \frac{1}{\zeta_1 - \bar{\zeta}_1} - \frac{\zeta_1}{1 - \bar{\zeta}_1^2} \right] \right. \\ & \left. + \frac{i\Gamma_{1s}}{2\pi} \frac{1}{\zeta_1(1 + \bar{\zeta}_1^2)} - s \frac{\zeta_1 + 1}{\zeta_1(\zeta_1 - 1)} \right\}, \end{aligned} \quad (3.4)$$

with the initial condition

$$\zeta_1(t_s) = \zeta_{1s}. \quad (3.5)$$

To close the problem we have to provide an equation for s which implements our control strategy. An ordinary differential equation for s can be obtained from (3.1) simply by setting $d\Gamma_1/dt = 0$, and $\Gamma_n = 0$, for $n = 2, 3, \dots, N$. Nevertheless, a simpler result follows from the fact that the problem of maintaining $d\Gamma_1/dt = 0$, $\forall t > t_s$, is equivalent to the problem of maintaining the Kutta condition satisfied when a vortex pair of fixed circulation is present in the flow. Then the suction which implements our control strategy is simply derived by solving (2.5) for s when $\Gamma_n = 0$, $n = 2, 3, \dots, N$. We have

$$s = -2U - \pi i \Gamma_{1s} \frac{(\zeta_1 - \bar{\zeta}_1)(1 - \zeta_1 \bar{\zeta}_1)}{(1 + \zeta_1^2)(1 + \bar{\zeta}_1^2)}. \quad (3.6)$$

A question arises about the compatibility of the equations (3.2) and (3.4). Compatibility is required to guarantee a smooth transition, at time $t = t_s$, from the final state of equation (3.2) to the initial state of equation (3.4). At time $t = t_s$ the Brown & Michael correction vanishes and the two equations coincide, consequently ensuring compatibility.

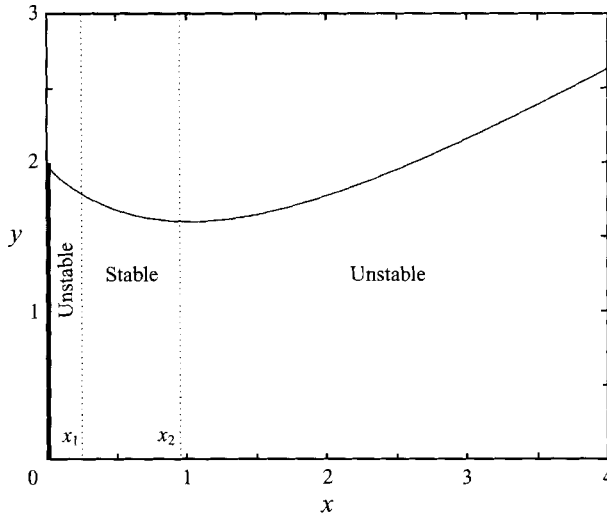


FIGURE 3. Locus of the fixed points.

4. Dynamical behaviour of the controlled system

In the previous section we have been able to find a controller which inhibits the production of circulation when a vortex pair is present in the flow. This section is devoted to the analysis of the dynamical behaviour of the controlled system.

As an initial step we solve for the fixed points of the unperturbed system. For convenience we rewrite equation (3.4) in polar form (see figure 1). We obtain

$$\frac{d\rho_1}{dt} = \frac{\rho_1}{\rho_1^4 + 1 - 2\rho_1^2 \cos 2\theta_1} \left[U\rho_1(\rho_1^2 - 1) \sin \theta_1 - \frac{s\rho_1^2(\rho_1^2 - 1)}{\rho_1 + 1 - 2\rho_1 \sin \theta_1} + \frac{\Gamma_1 \rho_1^2 [8\rho_1^2(\rho_1^4 + 1 - 2\rho_1^2 \sin \theta_1) \cos^2 \theta_1 - (\rho_1^4 - 1)^2] \sin \theta_1}{4\pi[(\rho_1^4 + 1)^2 - 4\rho_1^2 \cos^2 2\theta_1]} \cos \theta_1 \right], \quad (4.1a)$$

$$\frac{d\theta_1}{dt} = \frac{\rho_1}{\rho_1^4 + 1 - 2\rho_1^2 \cos 2\theta_1} \left[U(\rho_1^2 + 1) \cos \theta_1 + \frac{2s\rho_1^2 \cos \theta_1}{\rho_1 + 1 - 2\rho_1 \sin \theta_1} + \frac{\Gamma_1 \rho_1 (\rho_1^2 + 1) [8\rho_1^2(\rho_1^4 + 1 - 2\rho_1^2 \cos \theta_1) \cos^2 \theta_1 + (\rho_1^2 - 1)^4]}{4\pi(\rho_1^2 - 1)[(\rho_1^4 + 1)^2 - 4\rho_1^2 \cos^2 2\theta_1]} \right], \quad (4.1b)$$

where

$$s = \frac{\Gamma_1 s}{\pi} \frac{2\rho_1(\rho_1^2 - 1) \cos \theta_1}{\rho_1^4 + 1 - 2\rho_1^2 \cos 2\theta_1} - 2U. \quad (4.2)$$

Note that in the above equations the free-stream velocity is indicated with U for clarity although it is simply unity. Consequently, the problem depends only on one parameter, namely the circulation Γ_1 , of the vortex.

When suction is zero there is no vortex pair which is stationary and satisfies the Kutta condition, aside from the pathological situation where the vortex pair has infinite circulation and is infinitely distant from the plate. To the best of our knowledge there is no experimental evidence which contradicts this prediction. When suction is non-zero, there are fixed points and their locus is shown in figure 3. Each

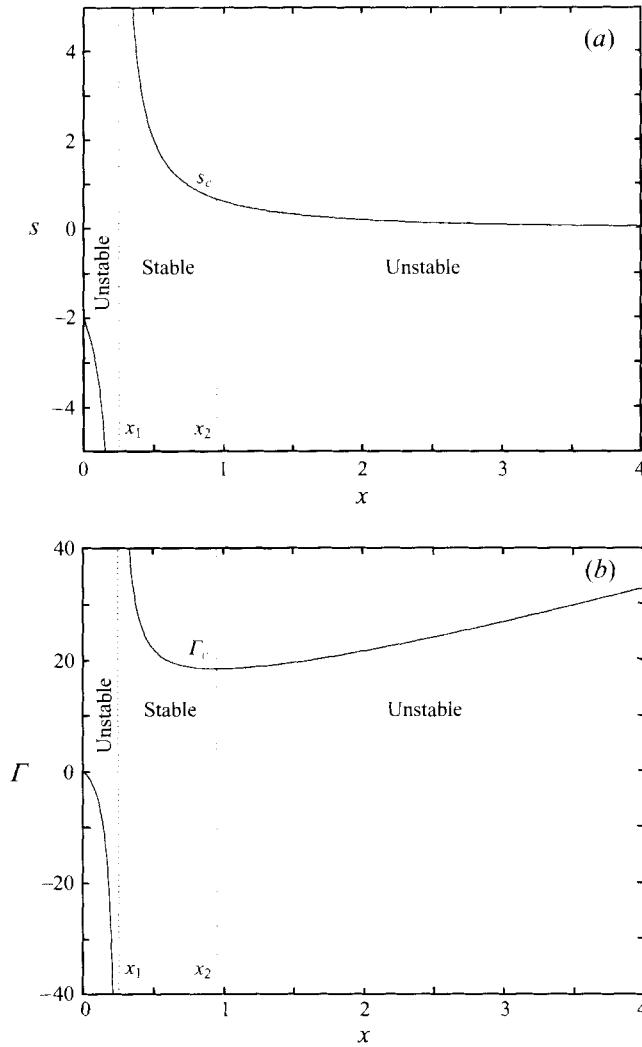


FIGURE 4. Suction (a) and circulation of the top vortex (b).

point on this curve represents the position of a vortex which is stationary and satisfies the Kutta condition, and whose circulation is shown in figure 4(b). The suction associated with each fixed point is shown in figure 4(a). The reader should be aware that we restrict our discussion to the upper half of the domain owing to the symmetry of the problem.

We derive a linear stability analysis to investigate the nature of the fixed points. Figure 5 shows the real and imaginary parts of the eigenvalues λ_1 and λ_2 . Three distinct regions can be recognized. Near the plate, where $0 < x < x_1$, the eigenvalues λ_1 and λ_2 are complex conjugates with positive real parts (see figure 5). In this region the fixed points are unstable foci. Figure 4 shows that both circulation and suction are negative. Physically it means that the Kutta condition is unusually satisfied by a vortex generating a counterclockwise flow and by injecting fluid. In particular, when $x = 0$, there are no vortices in the flow and the case shown in figure 2 is recovered. In the middle region, where $x_1 < x < x_2$, the eigenvalues are purely real

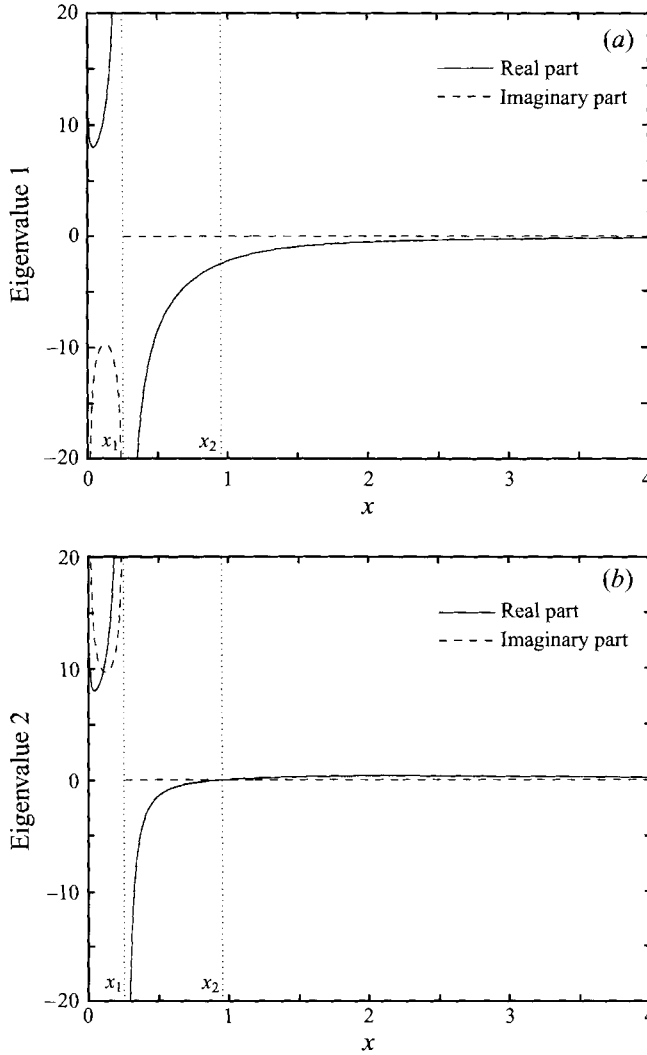


FIGURE 5. Real and imaginary parts of the eigenvalues λ_1 (a) and λ_2 (b).

with $\lambda_1 < \lambda_2 < 0$ (see figure 5). In this region the fixed points are stable nodes. Circulation and suction are both positive as expected (see figure 4). Note that the values of circulation and of suction at $x = x_2^-$ are the minimum values necessary to have a stable fixed point, that is $\Gamma_c \approx 18.49$ and $s_c \approx 0.67$ respectively. Note also that the asymptote at $x = x_1$ separates two regions with totally different dynamics. No smooth transition is possible between the two regions since both circulation and suction are discontinuous at $x = x_1$. In the third region, where $x > x_2$, the eigenvalues are purely real with $\lambda_1 < 0 < \lambda_2$ (see figure 5). In this region the fixed points are saddle points. As before, circulation and suction are both positive (see figure 4). The circulation increases from Γ_c to infinity while the suction decreases monotonically to zero as x goes from x_2 to infinity. Note that at $x = x_2$ the eigenvalue λ_2 is zero; this fact represents a sufficient condition for the bifurcation of a fixed point.

We restrict our discussion to the sub-domain where $x > x_1$, $\Gamma_{1s} > 0$, and $s > 0$. It is important to observe that in this sub-domain there are fixed points only when

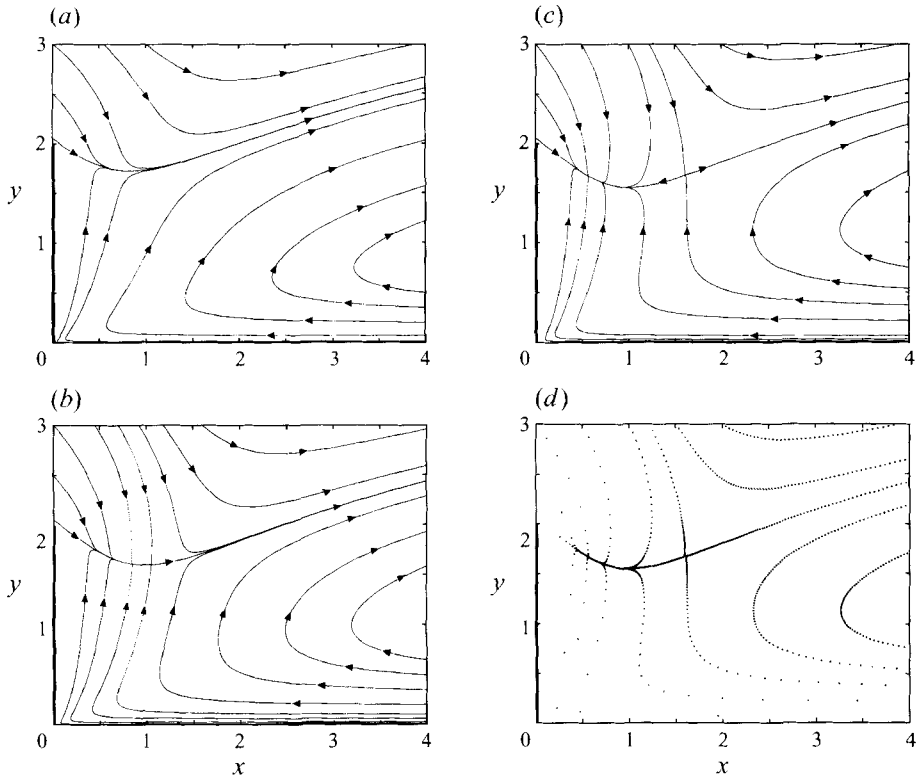


FIGURE 6. Vortex trajectories, $U = 1$: $\Gamma_{1s} = 15$ (a), $\Gamma_{1s} = 18.49$ (b), $\Gamma_{1s} = 20$ (c); Poincaré section, $U = 1 + \epsilon \sin(\omega t)$, $\epsilon = 0.1$, $\omega = 20\pi$, $\Gamma_{1s} = 20$ (d).

$\Gamma_{1s} \geq \Gamma_c$. As suggested by the behaviour of the eigenvalue λ_2 , the vector field undergoes a saddle-node bifurcation at $x = x_2$ when $\Gamma_{1s} = \Gamma_c$. Hence, the circulation Γ_{1s} plays the role of bifurcation parameter. Technically, the bifurcation should be analysed using the centre manifold theorem (see Guckenheimer & Holmes 1983, Chap. 4), but to maintain the paper focused on fluid mechanics we skip this formal step. To document the effect of the bifurcation parameter and to give a complete characterization of the dynamics of the system, we plot the sub-space of the phase space which coincides with the physical domain. In this plane the lines of flow of the vector field coincide with the trajectories of the vortex. The reader should be aware that these trajectories are obtained for constant free-stream velocity and circulation while suction in general changes along each trajectory. When $\Gamma_{1s} < \Gamma_c$ there are no fixed points. There are only two families of trajectories delimited by a separatrix (see figure 6a). When a vortex starts above the separatrix it drifts irreversibly downstream. When, instead, the vortex starts below the separatrix, depending on its initial position it can temporarily approach the plate, but eventually it drifts downstream. When $\Gamma_{1s} = \Gamma_c$ there is a non-hyperbolic fixed point and the flow pattern of the centre manifold can be easily recognized (see figure 6b). Finally, when $\Gamma_{1s} > \Gamma_c$ there are two hyperbolic fixed points: a stable node and a saddle point (see figure 6c). The vortex trajectory is characterized by the initial position of the vortex with respect to the stable manifold of the saddle point. If the vortex is initially on the left of the stable manifold, then it is driven by the controller to the stable node. It is interesting to observe that the trajectories between the stable manifold and the x -axis extend infinitely downstream.

When the vortex and its image are initially in the narrow region delimited by the stable manifold and the image manifold, they propel themselves upstream, and with the help of suction they first approach the plate and then are driven to the stable node and its image. When, instead, the vortex is initially on the right of the stable manifold it drifts downstream even if it temporarily approaches the plate. We define the controllability region as the basin of attraction of the stable node, i.e. the region delimited by the coordinate axes and the stable manifold of the saddle point. Note that as Γ_{1s} increases, the distance between stable node and saddle point also increases, with a consequent widening of the controllability region.

Since our final goal is to control the wake past the plate in the presence of an unsteady free-stream condition, it is crucial to investigate how the phase space changes under a time-dependent perturbation. The answer to this question is given by a theorem (see Guckenheimer & Holmes 1983, Chap. 4) which guarantees that the Poincaré section of a periodically perturbed system is topologically equivalent, for sufficiently small perturbations, to the phase space of the unperturbed system provided that the fixed points are hyperbolic. We perturb our system with a free-stream velocity of the form $U(t) = 1 + \epsilon \sin(\omega t)$ and compute the Poincaré section by plotting the vortex position at $t = 2n\pi/\omega$ for $n = 0, 1, 2, \dots$. The resulting Poincaré section presents two hyperbolic fixed points: a stable node and a saddle point, see figure 6(d). The stable node represents a limit cycle and the saddle point an unstable periodic orbit. As we show in the next section (see Figure 9b), the vortex is driven to a periodic orbit if it is initially on the left of the stable manifold of the Poincaré section. The topological equivalence between the phase space and the Poincaré section becomes evident by comparing figures 6(c) and 6(d). Because of this equivalence we can extend the definition of controllability region to the perturbed system. The controllability region coincides with the basin of attraction of the stable node of the Poincaré section.

In conclusion, suction is a powerful means of controlling the wake past a plate both in perturbed and unperturbed conditions provided that the vortex is initially within the controllability region. In the unperturbed case the vortex is driven to the stable node while in the periodically perturbed case it is driven to a periodic orbit.

5. Results

In this section we present the results of three simulations. The first two simulations document the ability of the controller to drive the vortex to the stable node when the free-stream velocity is constant, or to a limit cycle when the free-stream velocity oscillates periodically. The third simulation documents the performance of the controller when the free-stream velocity oscillates pseudo-randomly. In all simulations the initial evolution of the free-stream velocity was carefully chosen so that a vortex pair of nearly the same circulation $\Gamma_{1s} > \Gamma_c$ is shed in the flow at nearly the same time. Furthermore, suction is used to control the wake only after the rate of circulation production has gone to zero, i.e. when $t > t_s$, in order to provide the reader with an unbiased performance of the controller. In general, suction can be used to drive the system to a preferred state by the time $t = t_s$ when the controller takes over. Finally, all simulations have been terminated at $t = 10$ for editorial reasons although the controller could have performed successfully over any interval of time.

In the first simulation the free-stream velocity increases from rest, reaches a maximum value, and decreases to a unit value at $t = 1$ (see figure 7a). Three distinct time intervals can be recognized. Initially, when $0 < t < t_s$, the flow is uncontrolled and

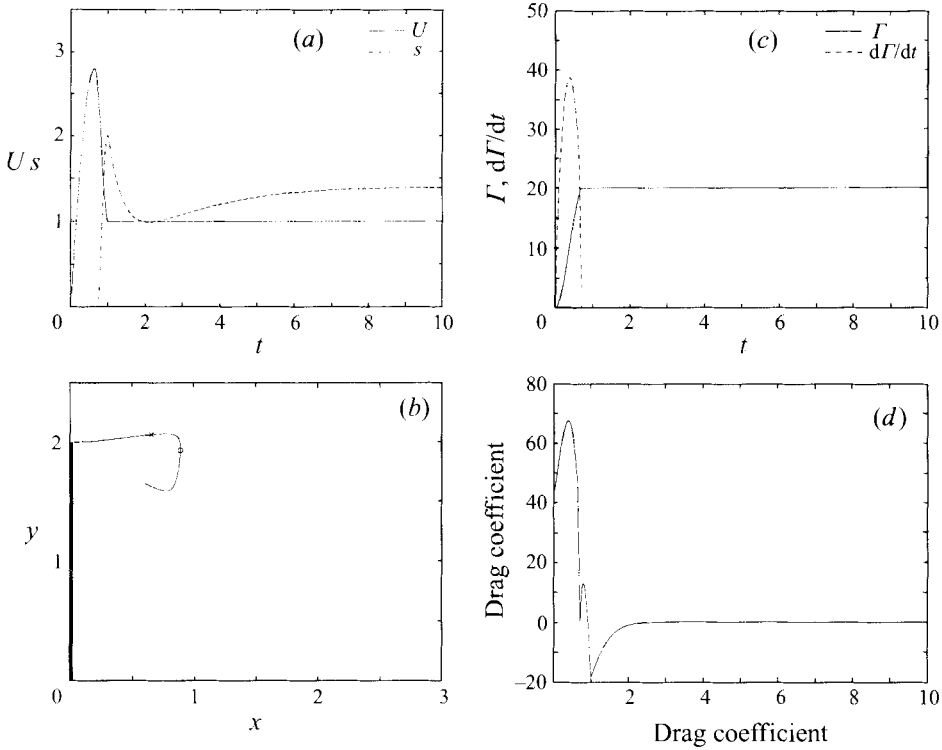


FIGURE 7. Simulation 1. (a) Free-stream velocity and suction. (b) Trajectory of the top vortex: \times , vortex position at $t = t_s$; \circ , vortex position at $t = 1$. (c) Circulation and rate of circulation production associated with the top vortex. (d) Drag coefficient.

separates from the tips of the plate, creating a vortex pair which drifts downstream. Figure 7(b) shows the trajectory of the top vortex. The rate of circulation production associated with the top vortex increases initially, decreases during the deceleration, and eventually becomes zero at $t = t_s \approx 0.71$ thereby triggering the controller (see figure 7c). At the same time the circulation of the top vortex reaches its maximum and final value (see figure 7c). The drag is dominated by the effect of the added mass because of the strong accelerations of the flow (see figure 7d). In the second interval, $t_s < t < 1$, the controller predicts the suction necessary to restrict the wake to a single vortex pair of constant circulation, $\Gamma_{1_s} = \pm 20.01$ (see figures 7a and 7c). The flow is still decelerating and the suction increases rapidly, driving the vortices away from their drifting trajectories and toward the x -axis (see figures 7a and 7b). The drag increases suddenly because of the effect of suction, but quickly decreases and becomes negative as the effect of the added mass returns to dominate (see figure 7d). Finally, when $t > 1$, the free-stream velocity and circulation are constants and suction drives the vortex pair to the stable node. Note that the vortex pair moves on the trajectory predicted by the analysis in §4 (see for a comparison figures 6c and 7b). The drag increases from its minimum value and eventually reaches a zero value as the added mass effect is subdued (see figure 7d). Figure 8(a–f) shows the instantaneous stream-function during the capturing process; because of symmetry we plot only the top half of the domain. Figures 8(a) and 8(b) show the flow at time $t < t_s$, where two recirculating bubbles grow and merge together. As suction becomes non-zero the recirculating bubble splits again into two bubbles (see figure 8c). Figure 8(c–f) shows

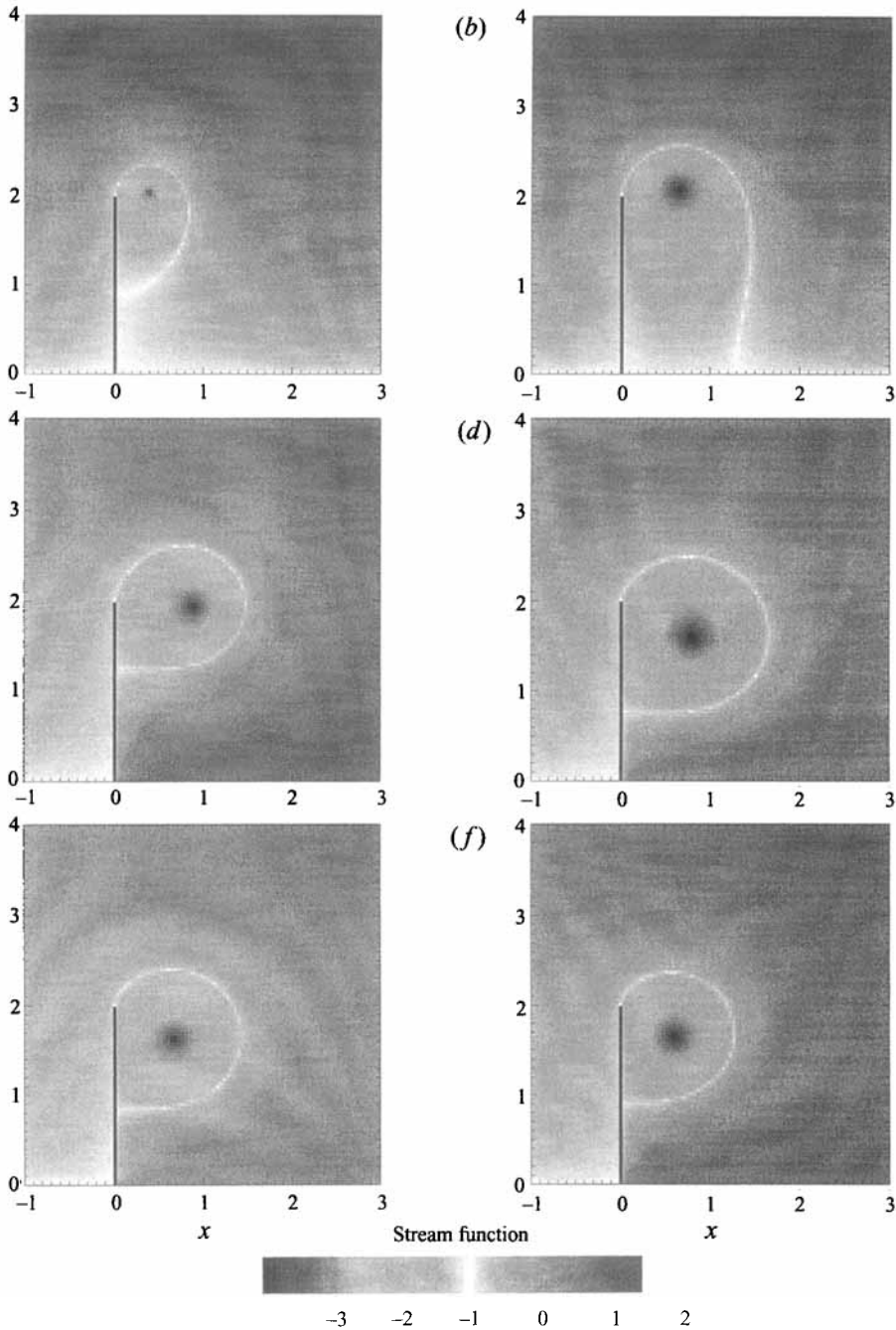


FIGURE 8. Instantaneous stream-function, $t = 0.51$ (a), $t = 0.71$ (b), $t = 1.02$ (c), $t = 2.02$ (d), $t = 4.02$ (e), $t = 8.02$ (f).

how the vortex is driven to the fixed point. Figures 8(e) and 8(f) are nearly identical because the flow has almost reached its steady state.

In the second simulation the free-stream velocity increases from rest and reaches a maximum value, as in the first simulation, but then oscillates about unit mean

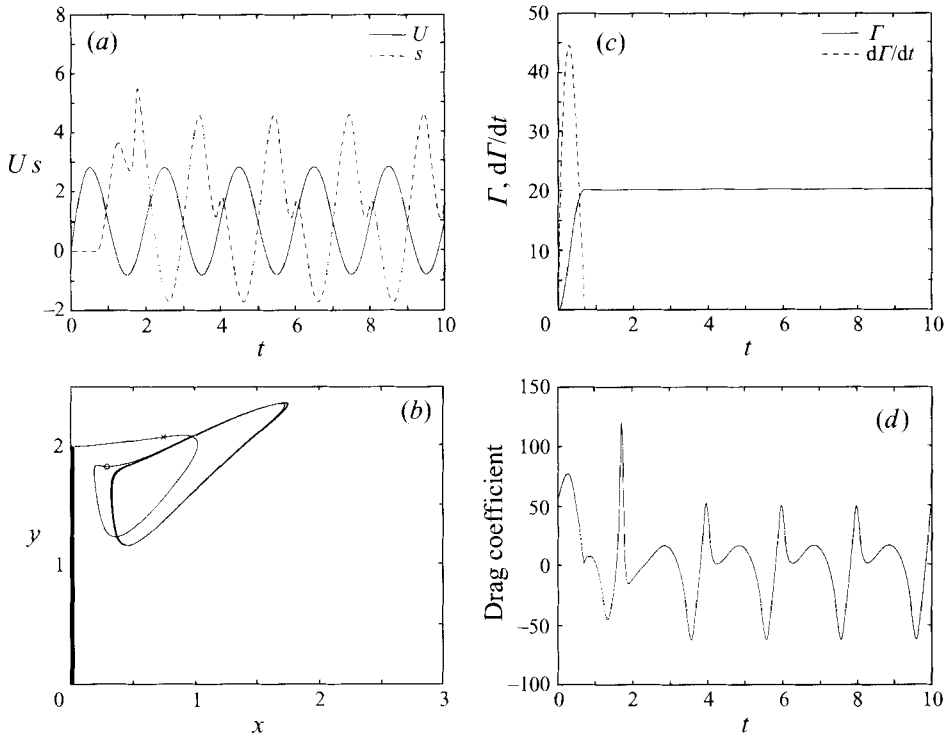


FIGURE 9. Simulation 2. (a) Free-stream velocity and suction. (b) Trajectory of the top vortex: \times , vortex position at $t = t_s$; \circ , vortex position after one period, $t = 2$. (c) Circulation and rate of circulation production associated with the top vortex. (d) Drag coefficient.

value (see figure 9a). Note that the amplitude of the oscillations is such that the flow reverses its direction for nearly one third of the period of oscillation, creating one of the worst possible scenarios for the controller. Three distinct intervals of time can be recognized. Initially, when $0 < t < t_s$, the flow behaves qualitatively as in the first simulation (see figure 9a–d). The rate of circulation production becomes zero at $t = t_s \approx 0.69$. In the second interval, $t_s < t < 2$, the controller predicts the suction necessary to restrict the wake to a single vortex pair of constant circulation, $\Gamma_1 \approx \pm 20.04$ (see figures 9a and 9c). Suction increases at first, then after a fluctuation it reaches its maximum absolute value, and finally decreases sharply. As a result the vortices are driven away from their drifting trajectories, at first toward the origin and then toward the tip of the plate. At the end of the first period the vortices are positioned near the limit-cycle trajectories (see figure 9b). The drag increases suddenly because of the effect of suction, then decreases because of the added mass effect, and finally presents a sharp peak because of the combined effects of flow acceleration and suction fluctuation (see figure 9d). Finally, when $t > 2$, all the flow quantities rapidly reach their final periodic behaviour while the circulation of the vortex pair is maintained constant, see figure 9(a–d). The vortices are rapidly driven to the limit-cycle trajectories where they orbit during the rest of the simulation, see figure 9(b). Figure 10(a–l) show the instantaneous stream-function during one period of oscillation, $6 < t < 8$, as the vortices move clockwise on the limit-cycle trajectories.

In the final simulation the free-stream velocity increases from rest and reaches a maximum value, as in the previous simulations, but then oscillates pseudo-randomly

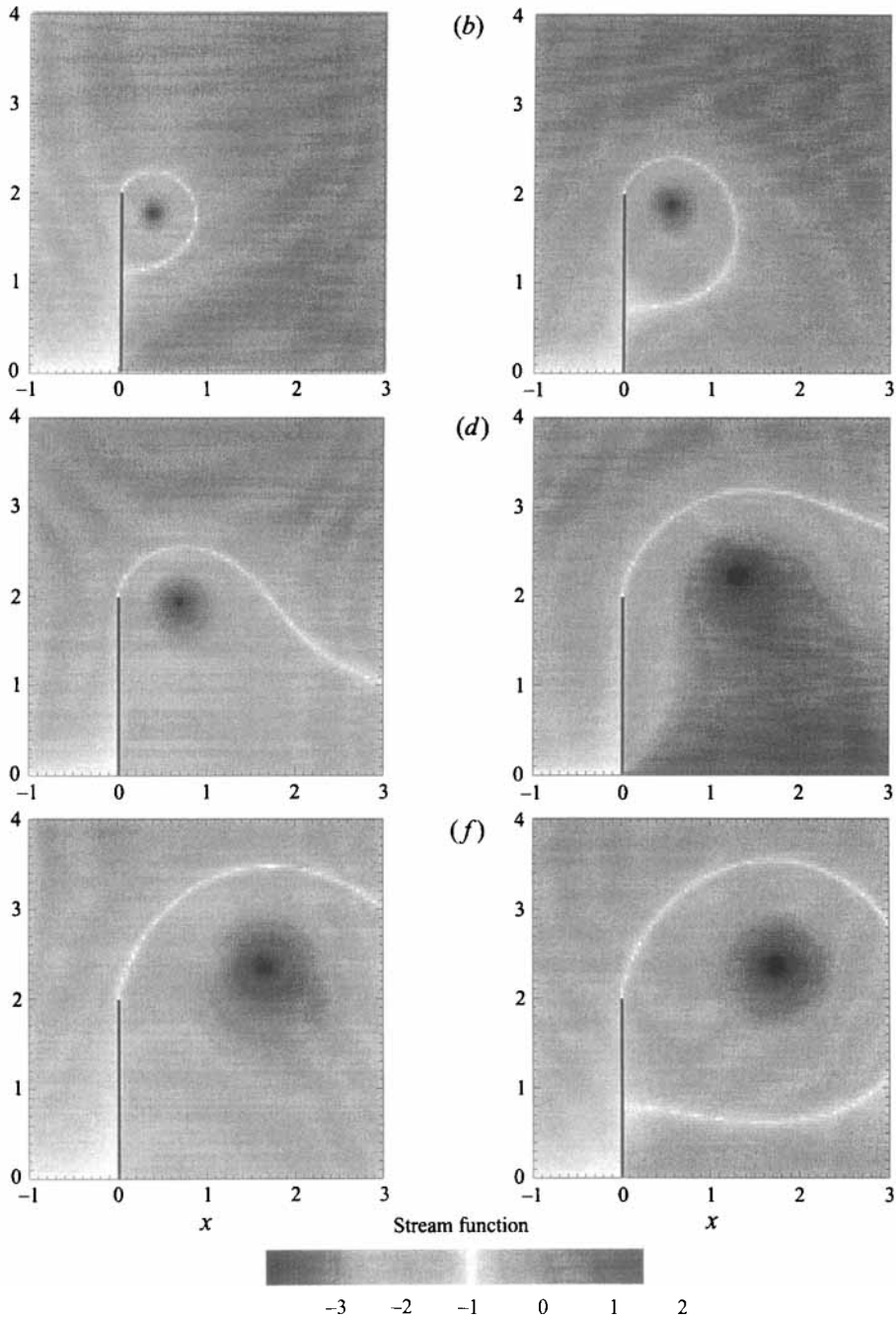


FIGURE 10(a-f). For caption see facing page.

about unit mean value (see figure 11a). Initially, when $0 < t < t_s$, the flow behaves qualitatively as in the previous simulations (see figure 11a-d). At time $t = t_s \approx 0.70$ the rate of circulation production goes to zero, triggering the controller which restricts the wake for the rest of the simulation to a single vortex pair of constant circulation, $\Gamma_1 \approx \pm 20.15$ (see figures 11a and 11c). Because of the pseudo-random character of the free-stream velocity it is difficult to give an interpretation of the time evolution

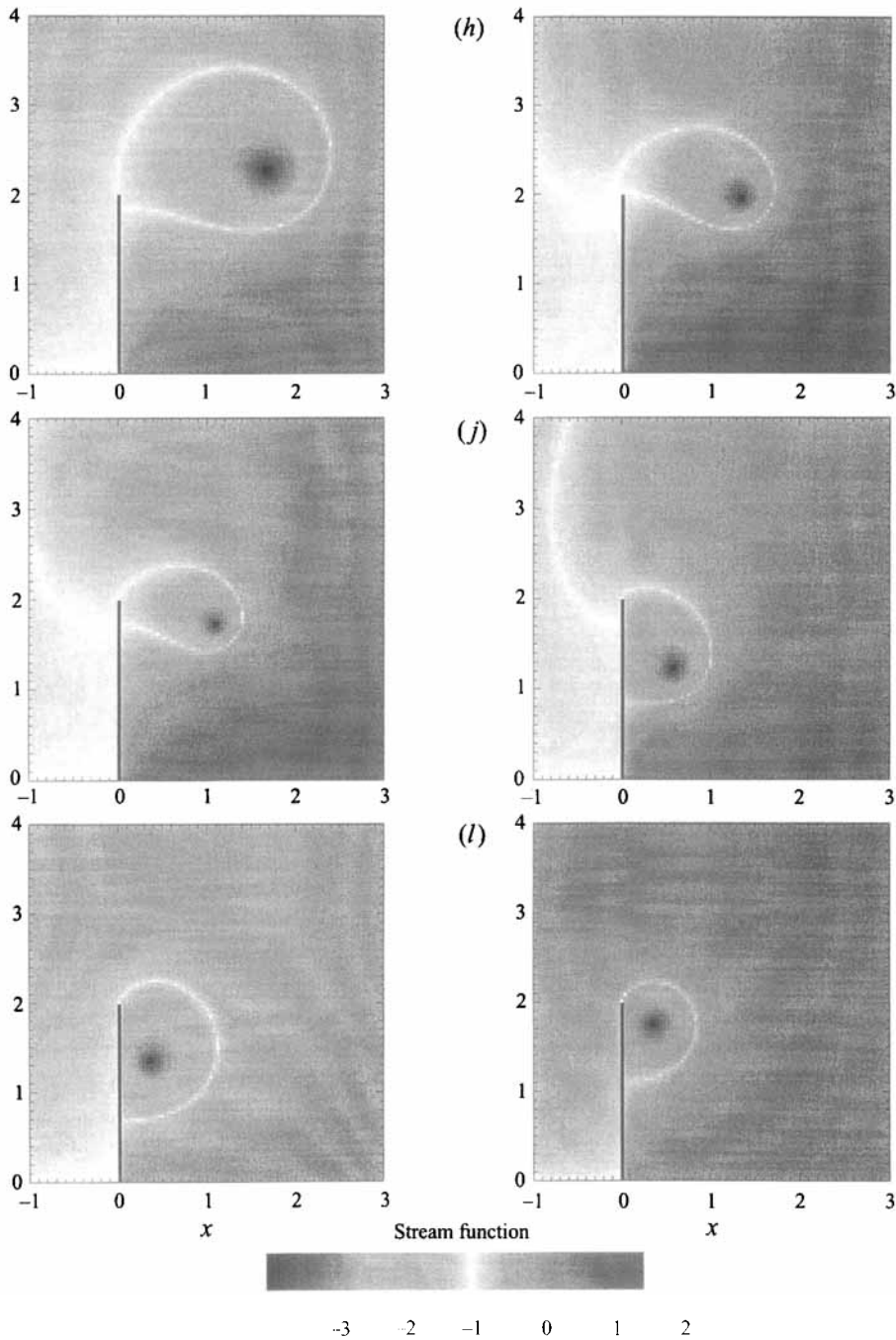


FIGURE 10. Instantaneous stream-function, $t = 6.05$ (a), $t = 6.25$ (b), $t = 6.35$ (c), $t = 6.66$ (d), $t = 6.86$ (e), $t = 6.96$ (f), $t = 7.16$ (g), $t = 7.36$ (h), $t = 7.46$ (i), $t = 7.67$ (j), $t = 7.87$ (k), $t = 8.07$ (l).

of suction in terms of the evolution of the flow. We can only say that suction is able to maintain the vortices orbiting on rather complex trajectories close to the plate. Note that the trajectories somehow entangle around the position of the stable nodes of the unperturbed system (see figures 6c and 11b).

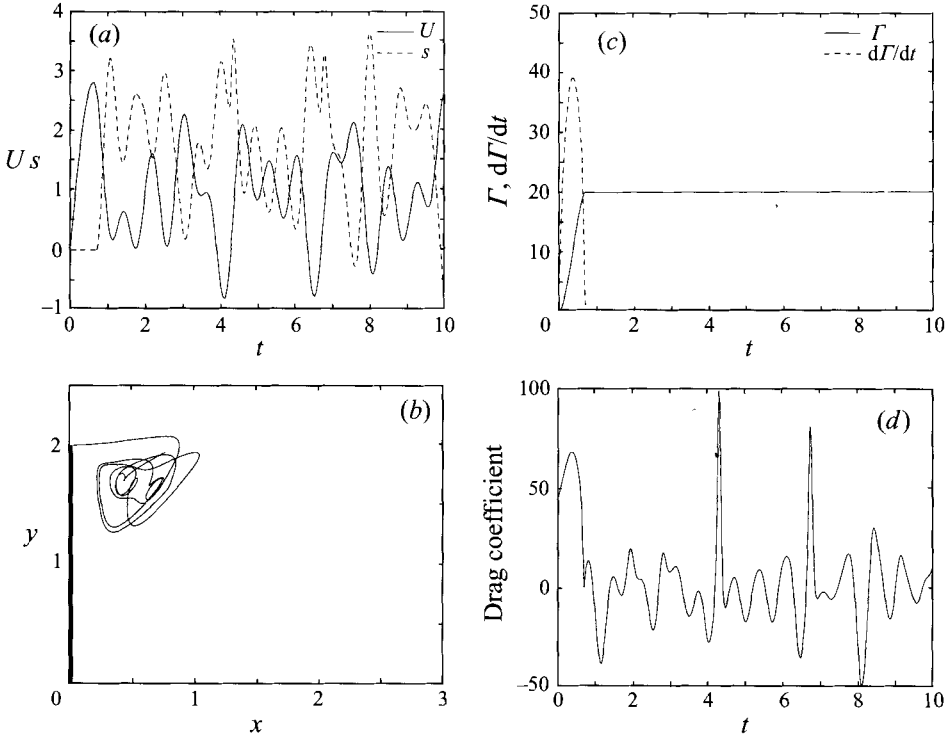


FIGURE 11. Simulation 3. (a) Free-stream velocity and suction. (b) Trajectory of the top vortex. (c) Circulation and rate of circulation production associated with the top vortex. (d) Drag coefficient.

Figures 9(a) and 11(a) might suggest to the reader that a simple phase shift of approximately π between the free-stream velocity U and suction s is sufficient for controlling the wake. In other words, the reader might wonder if a simple-minded linear controller which removes fluid when the flow accelerates and injects fluid when the flow decelerates can successfully replace the nonlinear controller derived in §3. This idea would imply that in the expression for the controller (3.6) the nonlinear term depending on the position and circulation of the vortex pair is negligible with respect to the linear term in U . As noted in §2 and showed in figure 2 the linear controller $s = -2U$ exactly controls an unsteady flow past a plate when no vortices are present in the flow. Consequently, the nonlinear term in expression (3.6) cannot be neglected. A careful analysis of figures 9(a) and 11(a) will show evidence of the effect of the nonlinear term.

6. Conclusions

A point vortex model has been used to simulate the unsteady separated flow past a flat plate with a suction point on the downstream wall. For this model we derived a control strategy that confines the wake to a single vortex pair of constant circulation. Owing to the simplicity of the model we obtained the analytical closed-form solution of the nonlinear controller for any free-stream velocity. The performance of the controller was characterized by a dynamical system type of analysis. In the case of steady flow the locus of the fixed points of the unperturbed system was computed. A pair of stable nodes and a pair of saddle points was shown to exist only if the

circulation associated with the vortex pair is above a critical value. It was also shown that the vector field presents a saddle-node bifurcation and that the circulation is the bifurcation parameter. The controllable region of the unperturbed system was identified with the basins of attraction of the nodes. In the case of unsteady flow the Poincaré section of the perturbed system was computed. Evidence of the topological equivalence between the phase space of the unperturbed system and the Poincaré section was presented. It was also shown that under perturbation the stable nodes of the unperturbed system become periodic orbits. The controllable region of the perturbed system was identified with the basins of attraction of the nodes of the Poincaré section. The predictions of our analysis were verified by testing the controller with three different unsteady free stream conditions. The first simulation documented the ability of the controller to drive the vortex pair to the stable nodes when the free-stream velocity is asymptotically constant. The second simulation documented the ability of the controller to drive the vortex pair to the periodic orbits when the free-stream velocity oscillates periodically about a unit mean. Finally, the third simulation showed the successful performance of the controller when the free-stream velocity oscillates pseudo-randomly about a unit mean.

The present study showed that the use of a reduced model provides a favourable environment to derive the desired control strategy and to test its performance and robustness. The natural continuation of the present work would be to embed the derived controller into a more complex and realistic model, for example the Navier–Stokes equations. The embedding process should be supported by a dynamical system and time series analysis to demonstrate the dynamical equivalence of the two models. Testing the controller in a different numerical environment instead of in an experiment presents several advantages. All the flow quantities required by the controller to command the actuator can be easily measured. The action of the controller is automatically synchronized with the evolution of the flow. Finally, the controller can be easily tested on gradually more complex flows allowing the researcher to make the controller progressively more robust with respect to different types of perturbations (e.g. viscosity, three-dimensionality, background noise, etc.). Successful completion of this process would open up the possibility of active control of large-scale coherent vortical structures in engineering applications.

The author wishes to thank Dr F. E. Marble for suggesting the use of a suction point as a means to control the flow. The author also wishes to thank Dr R. Camassa and Dr J. S. Gibson for several valuable discussions. This work was supported by the Air Force Office for Scientific Research Grant # F49620-92-J-0279.

REFERENCES

- BROWN, C. E. & MICHAEL, W. H. 1954 Effect of leading-edge separation on the lift of a delta wing. *J. Aero. Sci.* **21**, 690–694.
- CAO, N.-Z. & AUBRY, N. 1993 Numerical simulation of a wake flow via a reduced system. *Separated Flows*. ASME FED-Vol. 149.
- CHEERS, A. Y. 1979 A study of incompressible 2-d vortex flow past a circular cylinder. *Lawrence Berkeley Laboratory LBL-9950*.
- CLEMENTS, R. R. 1973 An inviscid model of two-dimensional vortex shedding. *J. Fluid Mech.* **57**, 321–336.
- CORTELEZZI, L. 1993 A theoretical and numerical study on active wake control. PhD thesis, California Institute of Technology.

- CORTELEZZI, L., LEONARD, A. & DOYLE, J. C. 1994 An example of active circulation control of the unsteady separated flow past a semi-infinite plate. *J. Fluid Mech.* **260**, 127–154.
- DOYLE, J. C. FRANCIS, B. A. & TANNENBAUM, A. R. 1992 *Feedback Control Theory*. Macmillan.
- FAN, M. K. H. TITS, A. L. & DOYLE, J. C. 1991 Robustness in the presence of mixed parametric uncertainty and unmodeled dynamics. *IEEE Auto. C.* **36**, 25–38.
- GAD-EL-HAK, M. & BUSHNELL, D. M. 1991 Separation control: review. *Trans. ASME I: J. Fluids Engng* **113**, 5–30.
- GRAHAM, J. M. R. 1980 The forces on the sharp-edged cylinders in oscillatory flow at low Keulegan-Carpenter numbers. *J. Fluid Mech.* **97**, 331–346.
- GOPALKRISHNAN, R., TRIANTAFYLLOU, M. S., TRIANTAFYLLOU, G. S. & BARRETT, D. 1994 Active vorticity control in a shear flow using a flapping foil. *J. Fluid Mech.* **274**, 1–21.
- GUCKENHEIMER, J. & HOLMES, P. 1983 *Nonlinear Oscillations, Dynamical Systems, and Bifurcation of Vector Fields*. Springer.
- KOCHESFAHANI, M. M. & DIMOTAKIS, P. E. 1988 A cancelation experiment in a forced turbulent shear layer. *First National Fluid Dynamics Congress July 25-28, 1988, Cincinnati, Ohio. AIAA Paper 88-3713-CP*.
- LISOSKI, D. L. 1993 Nominally 2-dimensional flow about a normal flat plate. PhD Thesis, California Institute of Technology.
- ONGOREN, A. & ROCKWELL, D. 1988a Flow structure from an oscillating cylinder. Part 1. Mechanisms of phase shift and recovery in the near wake. *J. Fluid Mech.* **191**, 197–223.
- ONGOREN, A. & ROCKWELL, D. 1988b Flow structure from an oscillating cylinder. Part 2. Mode competition in the near wake. *J. Fluid Mech.* **191**, 225–245.
- RAJAEI, M., KARLSSON, S. K. F. & SIROVICH, L. 1994 Low-dimensional description of free-shear-flow coherent structures and their dynamical behaviour. *J. Fluid Mech.* **258**, 1–29.
- RAO, D. M. 1987 Vortical flow management techniques. *Prog. Aerospace Sci.* **24**, 173–224.
- ROSSOW, V. J. 1977 Lift enhancement by an external trapped vortex. *10th Fluid and Plasmadynamics Conference, June 27-29, 1977, Albuquerque, New Mexico. AIAA Paper 77-672*.
- ROTT, N. 1956 Diffraction of a weak shock with vortex generation. *J. Fluid Mech.* **1**, 111–128.
- ROUSSOPOULOS, K. 1993 Feedback control of vortex shedding at low Reynolds numbers. *J. Fluid Mech.* **248**, 267–296.
- SHERMER, R. 1992 Control of vortex shedding in a two-dimensional flow past a plate. *Phys. Rev. A* **46**, 7614–7617.
- SLOMSKI, J. F. & COLEMAN, R. M. 1993 Numerical simulation of vortex generation and capture above an airfoil. *31st Aerospace Sciences Meeting and Exhibit, January 11-14, 1993, Reno, Nevada. AIAA Paper 93-864*.
- TOKUMARU, P. T. & DIMOTAKIS, P. E. 1991 Rotary oscillation control of a cylinder wake. *J. Fluid Mech.* **224**, 77–90.